Morphology-controlled precipitation of cerium oxalate crystals: The effect of water in nanostructured solvents

Irma Liascukiene, Marie Jehannin, Joseph Lautru, Renaud Podor, Sophie Charton, Fabienne Testard

Morphology-controlled precipitation of cerium oxalate crystals: the effect of water in nanostructured solvent

Irma Liascukiene[1]†, Marie Jehannin[3], Joseph Lautru[2], Renaud Podor[2], Sophie Charton[4], Fabienne Testard[1*]*

[1] Université Paris-Saclay, CEA, CNRS, NIMBE, 91191 Gif-sur-Yvette Cedex, France

[2] ICSM, CNRS, Univ. Montpellier, CEA, ENSCM, Bagnols-sur-Cèze, France

[3] ANU, RSPE, Department of Applied Mathematics, Canberra, Australia

[4] CEA, DES, ISEC, DMRC, Univ. Montpellier, Marcoule, France

Corresponding Authors: fabienne.testard@cea.fr and sophie.charton@cea.fr

†Present addresses: Laboratoire de Physique de La Matière Condensée, Ecole Polytechnique, CNRS, IP Paris, 91128, Palaiseau, France

Abstract

The ability to control the morphology of precipitated cerium oxalate material results in determinate evidence to its final properties. In this study, we demonstrate that surfactant free nanostructured low water solvents have a huge potential for controlling the morphology of a cerium oxalate powder. In this aim, an in-depth investigation of the reaction between cerium nitrate and oxalic acid is carried out, by varying both the relative concentration of the two reagents (around stoichiometric value), and the composition of the water / propanediol / octanol ternary solvent (especially in the low water-content nanostructured domain). Thanks to the complementary of observation methods: microscopy (confocal microscopy with fluorophores, environmental SEM), and X-ray scattering (SAXS, WAXS), we evidenced the role of the solvent on the growth kinetics and directional aggregation of the precipitates - the two major factors determining the final morphology of the particles. Besides the possible confinement effect in nanodroplets, compact "dense-branching" particles, achieved in low water content solvent, unveil the strong role of the surface forces on the aggregation mechanisms. This is consistent with the prevailing capillary forces at water / oil / solid triple points in ternary solvents. These new results confirm the high potential of nanostructured solvents for controlling the size and shape of hydrated precipitated particles.

Introduction

The control of powder morphology during precipitation has a huge interest due to the growing demand of functionalized materials in many industrial sectors such as pharmacy, ceramics and energy [1, 2]. However, while this route of synthesis is widely implemented industrially, the powder morphology obtained by precipitation remains difficult to predict and to control. Finding the appropriate manufacturing process, where functional performances demonstrated at the nanometric scale from laboratory synthesis are able to be reproduced at the industrial level, is a major technological barrier. It is especially of paramount importance today, for the economic viability of rare-earth elements (REE) recycling processes [3]. Controlling morphology is particularly challenging in the case of cerium-based particles for which the electronic structure, that influences the physical and chemical properties (such as intrinsic photoluminescence [4], biological activity [5] and catalytic properties [6]).

One of the simple, effective and low-cost CeO_2 synthesis routes is oxalic precipitation followed by a calcination step [7-10]. The process takes advantage of the high insolubility of oxalate salts to recover REEs. Ce^{III} salts and oxalic acid indeed easily and instantaneously co-precipitate in water solutions [11] following the global reaction:

$$2Ce(NO_3)_3 + 3C_2H_2O_4 + 10H_2O \rightarrow Ce_2(C_2O_4)_3 \bullet 10H_2O + 6HNO_3$$
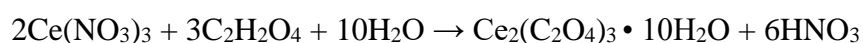
As for any crystallization process, the obvious lever to control the particles size is to manage the rate (ideally the mechanisms) of crystal formation. While near equilibrium, the growth of hierarchical structures highly depends on the origin of coordination complex between the metal and the ligand [12], randomly aggregated structures are obtained far from the equilibrium conditions [13]. Hence, studies first considered the effect of modifying the basic conditions of synthesis and mainly the supersaturation (changing temperature, acidity), the distance from equilibrium conditions (changing the initial reactant concentrations, the ratio between reactants) [14] and/or the viscosity of the reaction the medium [15, 16]. Large and high quality single

crystals have e.g., been grown by gel technique, where transport phenomena are dampened and where morphology and size can be tuned by pH of gel or the molarity of the strong acid solutions [17, 18].

On the other hand, monodispersed small (i.e., nano) Ce oxalate particles were obtained by confining the reaction within water droplets in microemulsions [19, 20], where surfactant, oil and water compositions can be seen as tunable parameters of the process. Vaidya et al. previously evidenced that implementing the reaction of Ce^{III} ions with oxalic acid in the aqueous core of micelles results in spherical agglomerated precipitates with size similar to the micelles (i.e., 4-6 nm) [20]. More recently, and accounting for the coordinating properties of the bidentate oxalate ion, that forms complex oxalates with the metal ion [21], the intrinsic properties of the solvent have been considered as a possible lever. Zhang et al. have tested different amino-acids crystallization modifiers to control the hierarchical nanoarchitectures [10]. Liu et al achieved the formation of 3D "flower-like" particles with high specific surface area, adding polyvinylpyrrolidone (PVP) in the Ce salt solution before its reaction with oxalic acid, in stoichiometric proportion [8]. Similar compact and organized cerium oxalate particles were synthesized by Jehannin et al. in over-stoichiometric conditions, and considering a ternary mixture of water, propanediol and octanol, with low water content [22]. One interesting feature of this ternary mixture is its nanostructuration that was revealed by SAXS.

In the last 10 years, a growing interest has been observed for this kind of nanostructured solvents, named as "surfactant-free microemulsions" [23], and more specifically for their Ouzo and pre-Ouzo regions [24, 25]. However, few papers report on their use for reactivity and nanoparticles synthesis [26, 27]. The structure of these ternary solvent (one hydrotrope in two immiscible solvents) used in [22], consists of embedded water-rich and octanol-rich pseudophases separated by a ultraflexible surface film [25] which is different from that of the microemulsion commonly used for nanoparticles precipitation [28]. Jehannin et al. were the

first to experiment them as precipitation medium for cerium oxalate particles [22]. Their results unambiguously relate the formation of various aggregated morphologies of cerium oxalate particles (including the microflowers) to the nanostructuration of the solvent.

The aim of this paper is to better understand this correlation and to highlight the involved mechanisms and from there to evaluate the possible tuning of the shape of precipitated cerium oxalate particles. We will particularly investigate the relative importance, and the respective role, of the growth and aggregation stages on the final cerium oxalate particles. Besides the differences in physical properties (as e.g., viscosity) likely to occur while moving in the ternary diagram, nanostructured solvents containing small amount of water exhibit interesting features for the control of the precipitation reaction. On one hand, the water-rich nanodomains, known as reversed pre-ouzo [29], can act as individual precipitation reactors (i.e. nano-confined precipitation) as in the micellar systems [20]. On the other hand, capillary forces that are particularly strong at the water/oil/solid triple points are likely to promote the bridging of the hydrophilic particles in the water-poor solvent, thus constraining them to form aggregates (i.e., capillary-induced precipitation) [22]. In this study, oil rich water / propanediol / octanol solvents with water contents as low as 10% have been prepared and characterized by small angle X-Ray scattering (SAXS) in order to further assess the influence of the water scarcity on the final morphology of the particles. In order to better discriminate how the solvent composition acts on the reaction mechanisms of cerium oxalate formation, and if possible, on their corresponding rates, we used a combination of complementarity microscopy techniques (optical, confocal microscopy and environmental SEM) and SAXS to characterize the morphology and the kinetic evolution of the particles. We chose a diluted cerium salt solution (i.e., 0.07M in the water domain, instead of 0.45M in our prior study [22]) in an attempt to reduce the apparent rates of growth and aggregation mechanisms.

The results will be discussed in 3 steps. First, the solvent structure is introduced, and its overall effect on the final particles' appearance is studied. In a second part, the effect of the oxalic acid concentration on i) the final morphology of the particles, and ii) on the course of the precipitation is examined, while the solvent composition is fixed. In the last part, different mechanisms are discussed to explain the proven effect of water-poor nanostructured solvents on the precipitation of cerium oxalate.

Experimental section

Materials and solutions

The precipitation reagents, cerium nitrate hexahydrate and oxalic acid with 99.99% minimum purity, and the solvent components, 1.2-propanediol ($\geq$ 99.5%) and 3-octanol (99%) were purchased from Sigma Aldrich.

Table 1. Composition (in mass fraction) of the tested solvents. The composition of the "oil rich solvent", ORS, used in [22] is reported for comparison. All cases represent monophasic ternary mixtures.

Name	% water	% propanediol	% octanol
ORS	24.70	55.30	20.00
Tern1	17.78	60.00	22.22
Tern2	9.76	65.85	24.39

Based on previous work, we prepared oil rich phases of water (Milli-Q, Millipore)/ 1,2-propanediol / 3-octanol [22]. We selected two different compositions with decreasing water content, down to approx. 10% (Table 1). The mixtures remained monophasic at room temperature.

The solutions of chosen concentration of each reagent were prepared in the same ternary solvent. All solutions stayed stable at room temperature when water is replaced either by an oxalic acid (at 0.070 to 0.535 M) or by a cerium nitrate water solution (at 0.070 M) (Table 2).

Table 2. Compositions of the tested reactive systems, where the concentrations for cerium salt and oxalic acid are given in the aqueous phase that replaces the water phase in the ternary system. The molar ratio ($Ce:C_2O_4$) is calculated for the ternary solution after mixing both reactant solutions (Ce^{3+} and $C_2H_2O_4$ ternary solutions) at $50/50_{v/v}$.

$2Ce(NO_3)_3 + 3C_2H_2O_4 + 10H_2O \rightarrow Ce_2(C_2O_4)_3 \cdot 10H_2O + 6HNO_3$						
$[Ce^{3+}]$, M of initial aqueous phase	**$[C_2H_2O_4]$, M of initial aqueous phase**	**$Ce:C_2O_4$ molar ratio in the total solution**	**Conditions**	**Sample name after precipitation**	**Sedimentation time in Tern1**	**Sedimentation time in Tern2**
0.070	0.070	1:1	unstoichiometric	$CeOx_{Unst}$	undetermined	-
0.070	0.105	2:3	stoichiometric	CeOx	$\approx$ 2-3 days	$\approx$ 7 days
0.070	0.315	2:9	excess	$CeOxEx_{1/2}$	undetermined	undetermined
0.070	0.535	2:15	excess	CeOxEx	$\approx$ 10 days	$\approx$ 16 days

The precipitation reaction was initiated by vortex-mixing together 50/50 volume of 500 µl of each reagent solution, (1st with oxalic acid and 2nd with cerium nitrate), during 2 minutes at the maximum speed. The solution turned white immediately, and sedimentation was observed after reaction, the time of sedimentation have been evaluated by eye. Additional experiments using water only as the solvent were also performed for comparison. We considered that reaction was completed when particles were fully sedimented at the bottom of the vessel (named as "final state"). The "after mixing" conditions describe the analysis on the mixture just after the 2 minutes mixing by vortex. Unless otherwise indicated, the precipitants were taken directly from the bottom of the vessel and analyzed without any washing step.
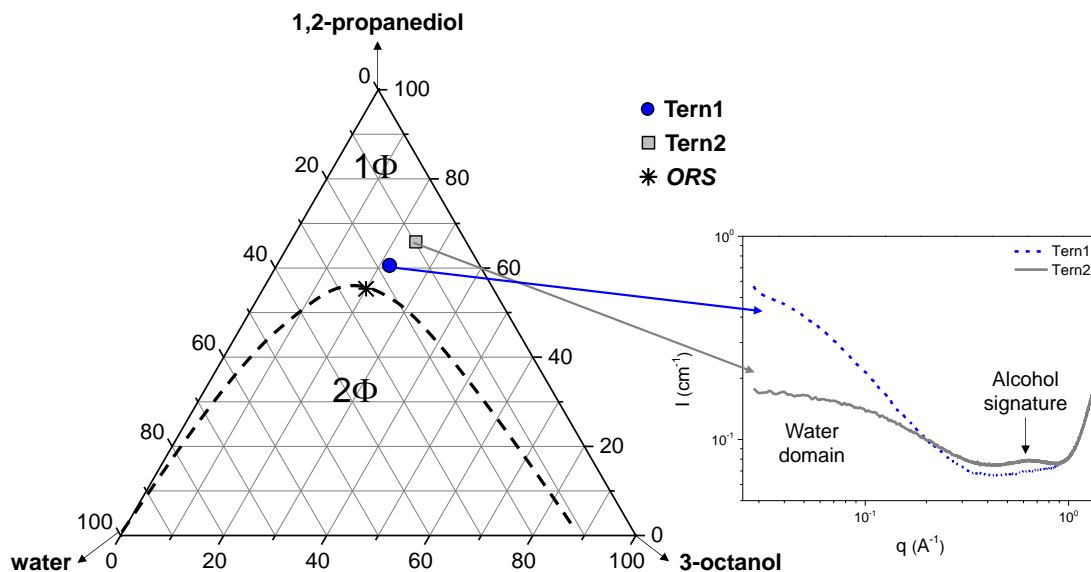
Figure 1. Left: The composition of ternary solvent is indicated in phase diagram of water/1, 2-propanediol/3-octanol: i/ Tern1 (wt/wt/wt% 17.78/60.00/22.22) is referenced by a blue circle, ii/ Tern2 (wt/wt/wt% 9.76/65.85/24.39) is referenced by a grey square, iii/ ORS, "oil rich solvent", used in [22] is referenced by a snowflake. All these conditions correspond to a monophasic domain at room temperature. Dashed line, as a guide for eyes, shows the limit between biphasic (below) and monophasic (above) phases following the phase diagram described by Jehannin [30]. Right: SAXS patterns of Tern1 and Tern2 solutions containing an oxalic acid/water solution for excess conditions.

Optical Microscopy

An inverted microscope (Leica DM IL) was used to observe continuously the precipitation reaction within a droplet deposited on the microscope glass slide. Images were acquired using a PIXELINK PL-B781U 6.6 MPixels camera.

The confocal images were taken with an Olympus Fluoview FV1000 inverted confocal laser scanning microscope. Samples of the crystals in ternary solvent (~60 µl) were placed in a quartz cell (0.5 mm light path) and examined at room temperature. The microscope is equipped with a laser with a wavelength of 543 nm, which excites Alexa Fluor™ 555 Carboxylic Acid, a tris(triethylammonium) salt (Molecular probes, Invitrogen, U.S.A.) soluble in aqueous phase

(identified in pink in the pictures) but not soluble in octanol phase. The fluorophore was added to the reactant before precipitation reaction, using the same quantity for each experiment.

Environmental Scanning Electron microscopy (ESEM)

An environmental scanning electron microscope Quanta 200 ESEM FEG (FEI Company) was used. When using the environmental mode, it enables to observe directly the particles in the liquid phase in which they form, by maintaining constant relative humidity around the sample. A Peltier cooling stage was used to maintain the sample temperature to 2°C, while the water pressure in the microscope chamber was adjusted to 708 Pa, i.e., exactly on the water liquid/gas equilibrium curve. Furthermore, a GSED (Gaseous Secondary Electron) detector was used to collect the electrons [31]. The images were recorded with an accelerating voltage of 6 kV. Two different conditions were analyzed. First, the samples were prepared in advance and the particles were studied by ESEM directly from the powder that has settled in the solution without additional washing (named as "final state"), and secondly by depositing a fresh reactive solution (named as "after mixing") directly on the sample holder.

Dried particles were prepared as described in "**SAXS/WAXS** *Ex situ*" part.

SAXS/WAXS

SAXS/WAXS data were acquired in SWAXSLab on a XEUSS 2.0 apparatus (XENOCS) in SWAXS Lab equipped with a Cu microfocus X-Ray source and a Pilatus (Dectris) 1M detector. The considered q-ranges from 0.0283 Å^{-1} to 1.350 Å^{-1} for Tern 2 and 0.0356 Å^{-1} to 2.300 Å^{-1} for Tern1 are obtained from a single sample to detector distance (45.0 cm Tern2 and 24.5 cm for Tern1 respectively). The q-ranges are calibrated with tetradecanol. The detector count is normalized from a direct beam measurement and the Standard procedures were applied to subtract background scattering and to normalize the intensities using an in-house extension of an open-source Python SAXS software [32, 33].

Ex situ

Samples were prepared following the protocol described in *Material and solutions* part. They were quenched by centrifugation after chosen reaction-times: 4h, 1-3days. The solvent traces are supposed to be removed by repeating centrifugation 3 times and by washing the collected solids with ethanol. The obtained powder was analyzed on a sticky Kapton film after being dried at room temperature. The acquisition time is 1800 s for each powder and each configuration.

In situ

Samples were prepared following the protocol described in *Materials and solutions* part. Just after mixing, borosilicate capillaries (VJM-Glas/Müller GmbH) of 1.5 mm thickness are filled, sealed, and measured for different reaction times to follow the kinetic of the formation of particles before their sedimentation, when it occurs. The acquisition time is 1800s for each measurement, and for the two sample to detector distances.

Results and Discussion

Structure of the synthesis media and its overall effect on the appearance of the cerium oxalate crystals

The nano-organization of the Tern1 and Tern2 ternary solvents was characterized by SAXS, that reveals different nanostructures. Figure 1 shows the SAXS patterns obtained for both ternary systems when containing oxalic acid in excess conditions. In the large q-range, the broad peak around 1.4 Å^{-1} combines the signature of the liquid alkane chains and water. The broad peak at 0.64 Å^{-1}, mainly visible in Tern2 solution is a characteristic correlation peak classically observed for alcohols [34], here it is related to the propanediol-octanol mixture. Finally, the signal in the small q-range is characteristic of the presence of globular domains with higher

electronic density than alkane chains, as already evidenced in the water/propanediol/octanol ternary mixtures [22], and typical of ternary solutions containing one hydrotrope and two immiscible fluids [25]. The SAXS signal is slightly modified depending on whether the aqueous phase is pure water or a cerium nitrate solution instead of the oxalic acid solution (see Figure S1). The curves can be fitted for the water case by either a Gaussian distribution of spheres for Tern 2 (R= 4.0 Å, σ= 4.0), or by cylindrical shapes with ellipsoid section (of aspect ratio AR) for Tern 1 (R= 5.7 Å, AR=2.0, L= 103.0 Å) (See figure S1). These domains contain the water and OH groups from the alcohols, they are of bigger size for Tern1 than for Tern2. The differences in domain's size mainly come from the water content in the water/propanediol/octanol ternary system. We can conclude that if nanostructuration has an impact on the reactivity of cerium oxalate precipitation, the water content is an important parameter.

The synthesis of cerium oxalate in ternary system is obtained by mixing in volume-to-volume ratio the two ternary reactant solutions containing cerium nitrate and oxalic acid (see Table 2 for composition). For the excess oxalic acid case, a simple observation by eye indicates that a longer time is required after mixing to reach sedimentation of the particles in the ternary system in comparison to water (10 days, 16 days and few seconds, respectively for Tern1, Tern2 and water). The ESEM observation of the sedimented particles also indicates differences. The particles from ternary solutions appear rather as separated units compare to those from water solutions, and their size and branching increases as the water content is decreased (Figure S2), while the infrared signatures of the precipitates are similar (Figure S3), meaning the composition is the same. Going from pure water to ternary alcohol solutions modifies the viscosity of the solution. This is associated to a reduction of the particles sedimentation rate, and most probably aggregation between them, but also to a modification of the reactivity by changing the local transport properties. Both phenomena are consistent with the observed

morphology modifications. We thus turn to investigate the impact of the stoichiometry on the final morphology achieved with the 3 solvents (Tern1, Tern2 and water) in an attempt to better assess the role of solvent composition in reactivity and morphology.

Impact of the oxalic acid concentration on the precipitation of cerium oxalate. Case of Tern1 solvent

The range of oxalic acid concentrations considered for the synthesis of cerium oxalate in ternary solvent Tern1 is indicated in Table 2.

Final morphology

ESEM images show that the final products obtained at the end of the precipitation reaction exhibit different morphologies, depending on the oxalic acid concentration (Figure 2). Note that we here present the results obtained in the Tern1 system, although, as it will be illustrated in the second part of the article, the same trends were observed in the Tern2 system.

For stoichiometric conditions ($Ce:C_2O_4 = 2:3$) (Figure 2, CeOx) the reaction results into 30 µm diameter compact cross-like crystals with ≈ 6 µm thickness; the blocks of platelets unfold into 45° or even smaller angles by creating the shape of fans or micro-flowers, as they were named by Liu et al. [8].

Using a complete excess of oxalic acid ($Ce:C_2O_4 = 2:15$) (Figure 2, CeOxEx) on the other hand leads to the formation of less compact aggregates with thin and long platelets and rods. The branches arranged themselves in a less regular pattern, creating long crosses or sort of "sea urchins" (length = 25 µm, thickness of platelets ≈ 0.5 µm) for the more complex assemblies, while being connected by their center.

At intermediate over-stoichiometric oxalic acid concentration ($Ce:C_2O_4 = 2:9$) (Figure 2, CeOxEx$_{1/2}$), a mixture of compact microflowers, observed in stoichiometric conditions, and of the loose "sea urchins", typical of strong oxalic excess, is found.

For under-stoichiometric conditions (Ce:C_2O_4= 1:1) (Figure2, $CeOx_{unst}$), a mixture of small platelets, with length l=3.5 µm, and compact crosses of diameter around 18 µm, is observed. The angle at the intersections of two blocks is 90°, suggesting that the microrods could first assemble perpendicularly or grow in two opposite directions separated by a 90° angle.

The obtained evolution of the particles shape with the oxalic acid concentration is consistent with the previous observations where, at a oxalic acid / cerium nitrate ratio of 1.6 (Ce:C_2O_4=1:1.16), a sharp transition from compact micro-flowers, synthetized at lower oxalic excess, to less compact aggregates (needles in the more extreme cases) at higher oxalic excess was observed [30]. Smaller particles, but with similar morphologies were also evidenced in PVP-aqueous solutions, where micro-flowers (2-3µm) form at stoichiometric conditions, whereas irregular branchlike microrods (7-8 µm) form when oxalic acid is in excess, and two-micron size rods crossed together precipitate for under-stoichiometric conditions [8]. Star-like assemblies of needles have also been observed after synthesis of cerium oxalate in pure water, at low temperature, with acidic conditions and for a specific pathway for reactant addition (cerium salt added in oxalic acid) which correspond to an excess of oxalic acid during the synthesis [14].

The ESEM pictures that are reported in Figure 2 indicate that in the nanostructured solvent Tern1, as in aqueous solutions, the higher the distance from stoichiometric conditions (here represented by the excess of oxalic acid), the higher the branching of the aggregates, and the smaller the thickness of the "elementary" platelets and rods. This behavior is consistent with the one known in water solvent. However, the final size achieved by the particles in structured solvents is bigger (25µm – 30µm).

CeOx_unst

CeOx

CeOxEx_1/2

CeOxEx
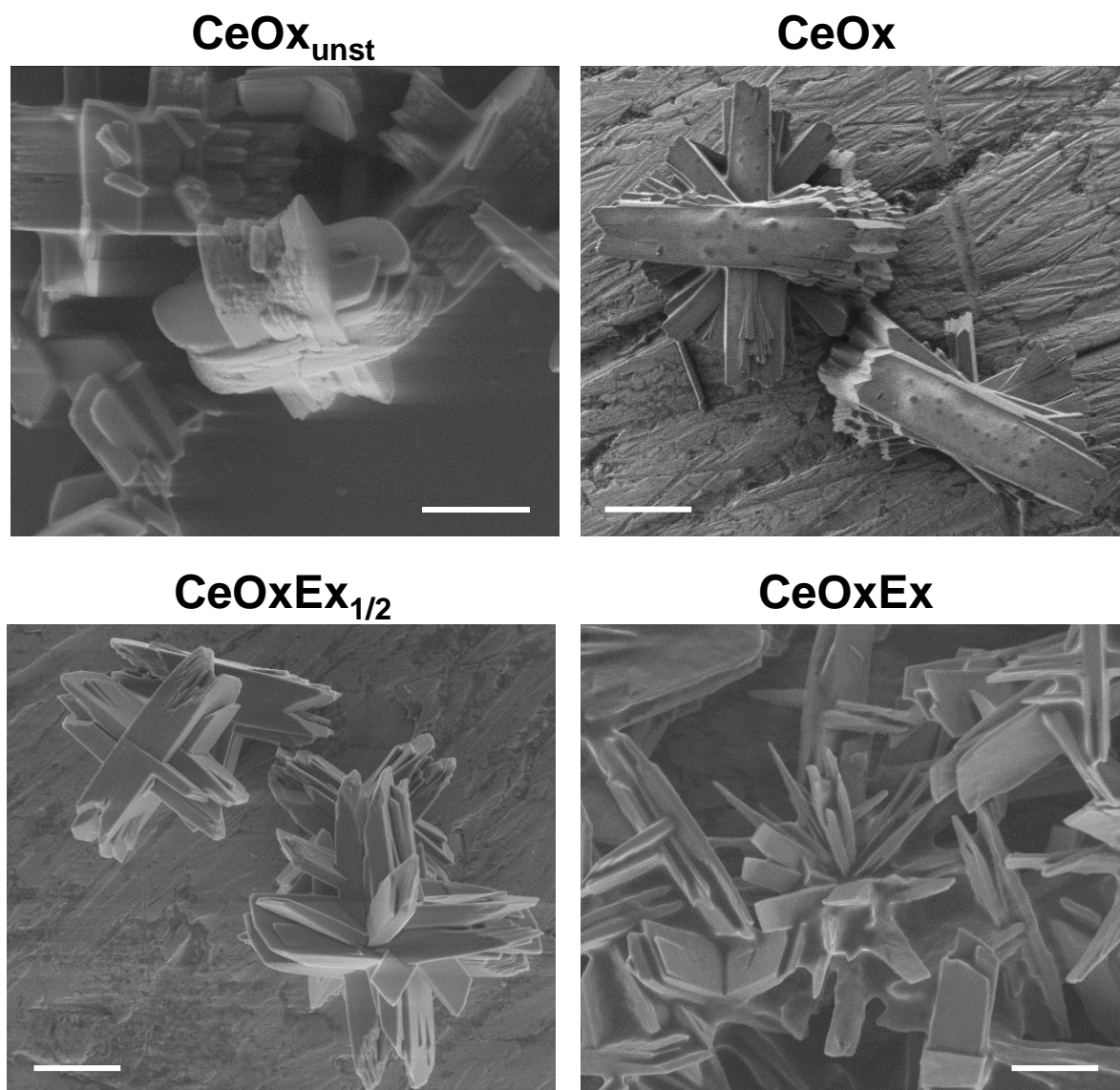
Figure 2. Morphology of cerium oxalate crystals at the "final state" after their synthesis in ternary solvent **Tern1** for different concentrations of oxalic acid: 0.070M (CeOx$_{Unst}$, Ce:C$_2$O$_4$=(1:1)), 0.105M (CeOx for stoichiometric conditions, Ce:C$_2$O$_4$=(2:3)) ("microflowers"), 0.315M (CeOxEx$_{1/2}$, Ce:C$_2$O$_4$=(2:9)), 0.535M (CeOxEx, Ce:C$_2$O$_4$=(2:15)) ("sea urchin"). Scale bars are 10μm.

Progress of the precipitation process

In Tern 1 system, for all conditions (different Ce:C$_2$O$_4$ ratio), reaction was immediate and the mixture instantaneously turned white as the solutions of cerium nitrate and oxalic acid got into contact. In a view of highlighting the detailed growth mechanisms responsible for the final achieved shape, and in particular the nature of the first "grains" responsible for the whitish

coloring appearing just after mixing, ESEM and optical microscopy were used to investigate the time-evolution of the crystals (Figure 3 and Figure S4).

ESEM. Droplets of solution just after mixing or (visible powder + solution) obtained after 1 day are introduced in the microscope for observation. For stoichiometric conditions, homogeneous size and shapes (named as "sandwiches" or brick-like) were observed just after mixing with the following typical dimensions: length l=3µm, width w=2µm and thickness t=1.5µm (Figure 3A). Homogeneity of the particles' population is highlighted in Figure S5. Many sandwiches exhibit protrusions getting out from the side plane (nail shape, inset of Figure 3A), which probably are prime growth sites to achieve the final cross shape of Figure 3C. Some tiny crosses were even observed at this early stage. Zooming more, smaller platelets, with a length l=0.5-0.7µm, were observed in coexistence with the other shape (Figure 3B, Figure S6 B), that could be the primary species for these stoichiometric conditions. Similar structures, and particularly the nail shape, and small platelets, have been observed prior to the drying of the solvent (see Figure S6A), hence confirming the process leading to the typical morphology obtained for stoichiometric precipitation in Tern1 appears rapidly and before the growth phase.

With an excess of oxalic acid, the elapsed time between the reactants mixing and the complete sedimentation of the particles was significantly longer than for stoichiometric conditions, (approximately 3 times longer regarding the sedimentation times only). Paradoxically, the particles observed just after mixing were much larger than those synthetized in stoichiometric conditions (Figure 3 D and E, Figure S6 C). Two types of shapes predominate: *i)* long crosses folded aside by 2-3 stacked platelets, which could unfold to achieve the shape of snowflakes (angle, where two blocks intersected, is 90°, the length of both parts was around 10 µm); and *ii)* pins (length of longer part was round 10 µm, length of the shorter part was around 5 µm, half of the diameter of the full cross) evocating the rapid growth of the ends of the sandwich-shape with protrusions observed in stoichiometric conditions. The less compact morphology of

15

these particles achieved far from equilibrium, when compared to the particles obtained under stoichiometric conditions, can explain their slower sedimentation.
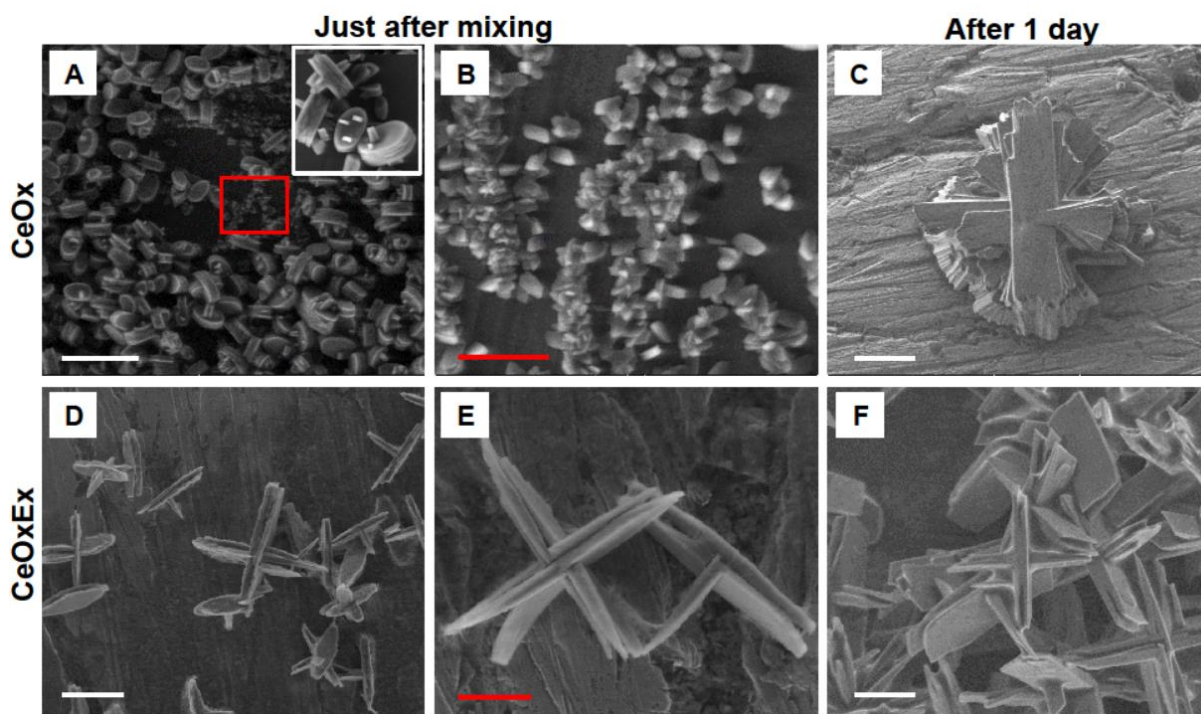
Figure 3. Environmental electron scanning microscopy (ESEM) of cerium oxalate particles under stoichiometric conditions (A, B, C) and excess of oxalic acid (D, E, F) synthetized in ternary solvent **Tern1** just after mixing (A, B, D, E) and after 1 day (C, F). The same precipitant solution (CeOx and CeOxEx, independently) was taken for the observation of the evolution of particles' morphologies just after mixing and after 1 day. The inset, in the white square, is a zoom to better demonstrate the morphology of the particles. The red rectangle in A is the region of interest for the bigger magnification presented in B. Scale bars are 10 µm (A, C, D, F) and 3 µm (B, E).

Optical microscopy. The observed difference in morphology was also observable after 3 hours, directly on the reactive solutions (i.e., without the evaporation step required by ESEM), thanks to optical microscopy. The bright field images confirmed that two different characteristics shapes are achieved depending on the initial oxalic acid conditions (Figure S4): "crosses" and "snowflakes" for stoichiometric ratio of reactants (Figure S4 A), and for excess of oxalic acid (Figure S4, D), respectively, which further continue to evolve (Figure S4 B, C, E, F).

From ESEM and optical microscopy, we can conclude that the orientation towards final morphology is visible after mixing, materialized by thick and compact particles for stoichiometric conditions and by thinner and branched particles for oxalic excess conditions. Additional *ex-situ* and *in-situ* analysis were implemented to consolidate these qualitative microscopy observations.

Complementary *ex situ* analysis. The particles precipitated in the Tern 1 solution were characterized by means of *ex situ* SAXS/WAXS and ESEM analyses for two reaction times (4 hours and 3 days) (Figure 4). Contrary to the conditions used in Figure 3, particles have been separated and washed before their observation. This means that under ESEM, no excess of reactant is present during the drying process in the microscope. The reaction times were selected to catch the morphology and structure of the particles under evolution, knowing that after 3 days, the particles have fully sedimented for the stoichiometric conditions and not completely sedimented for the excess conditions. After 4h, the extracted crystals from stoichiometric condition exhibit several Bragg peaks typical of cerium oxalate decahydrate crystallographic structure (monoclinic structure with lattice parameters a = 11.34 Å, b = 9.630 Å, c = 10.392 Å and β= 114.5° (JCPDS Card No 20-0268)), while for those produced in excess oxalic acid conditions the Bragg peaks typical of cerium oxalate (0.61 Å^{-1}, 1.26 and 1.30 Å^{-1}) are small and in coexistence with another Bragg peak at 0.98 Å^{-1} and a broad peak at 1.21 Å^{-1}. Other crystal structures in coexistence with the cerium oxalate are thus visible for the excess oxalic acid conditions. The Bragg peaks at 0.98 Å^{-1} can be related to the (100) orientation of hydrated oxalic acid crystals (close to expected Bragg peak from monoclinic structure with lattice parameters a=6.12 Å, b=3.61 Å, c=12.03 Å and β=106.12°). This means that oxalic acid crystals are trapped in the cerium oxalate precipitates, as it is not removed by the washing steps, although highly soluble in ethanol. The other broad peak at 1.21 Å^{-1} could be related to an intermediate amorphous state, which is only visible for excess conditions. Therefore, for the

excess conditions, the *ex situ* SAXS evidences intermediate structures (oxalic acid crystal and an amorphous phase) in coexistence with the cerium oxalate crystal in formation.

After 3 days, the positions of the Bragg peaks are the same for the two conditions indicating that the precipitates exhibit the same crystallographic structures typical of cerium oxalate. However, for the excess conditions, the Bragg peak centered at 0.61 Å^{-1} and related to the (100) facet of cerium oxalate decahydrate is the most intense contrary to the stoichiometric conditions. The excess oxalic acid conditions favored the growth of the (100) facet.

From ESEM, we also observe differences in the particle morphologies for the 2 reaction times (4 hours and 3 days), with compactness for stoichiometric conditions and branching for excess of oxalic acid. These findings are in agreement with the observations on the reactive solutions after mixing and after 1 day (Figure 3 and Figure S4), and with those on the final state after complete sedimentation (Figure 2).
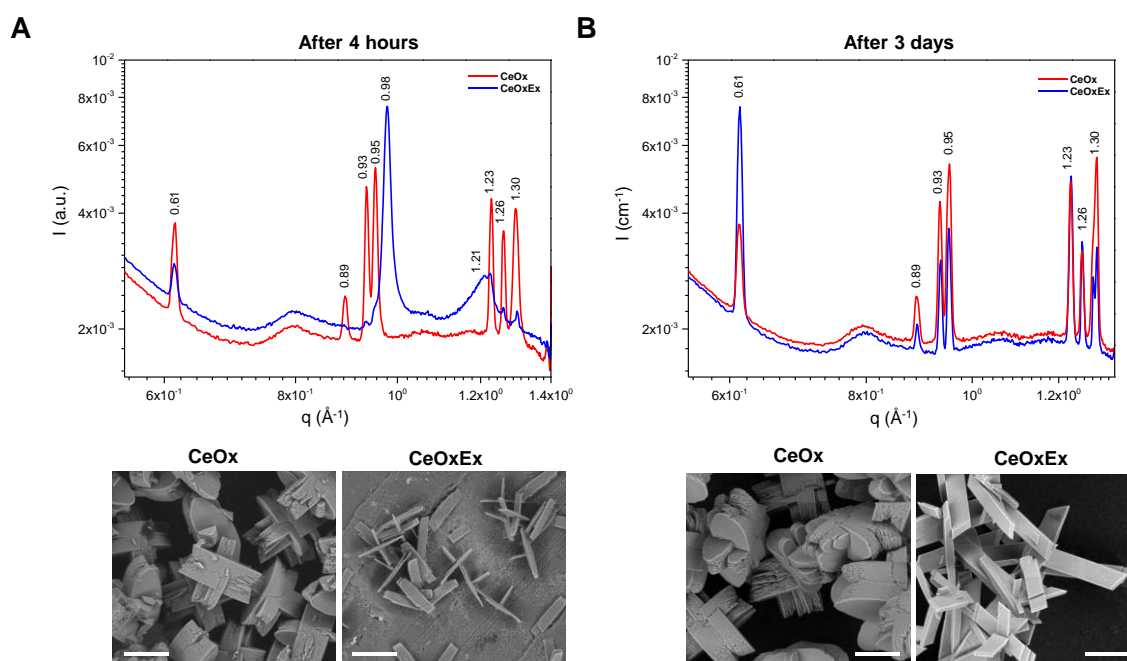

Figure 4. WAXS data *ex-situ* of the cerium oxalate particles under stoichiometric conditions (CeOx) and excess of oxalic acid (CeOxEx) in ternary solvent **Tern1** with the corresponding images of

environmental electron scanning microscopy (ESEM) after (A) 4 hours and (B) 3 days after centrifugation and washing steps. Scale bars correspond to 10 µm.

Complementary *in situ* analysis. In order to follow the crystal growth in the Tern1 ternary system, the ageing of the solution was monitored by SAXS after the mixing of the two reactants considering stoichiometric (CeOx) and excess of oxalic acid conditions (CeOxEx). The SAXS intensity due to the particles is well above the ternary solvent ones (see Figure S7), with one to two decades of difference in intensity in the low-q region. In the large q-range, the signature of the ternary solvent comes from the nature of its components and is defined by a correlation peak due to water and alcohol organization. We thus have subtracted the ternary solvent signal from each curve acquired during the kinetic experiments, to extract the signature from particles growth and crystallization (Figure 5 and Figure S8, S9). The high scattering signal in the low q-range is the signature of the size (diameter, 2R) and density number (N) of the growing constitutive particles embedded in bigger grain, while the gradual appearance of the Bragg peaks in the large q-range is characteristic of the crystallization process of the particles.

In situ SAXS provides more indications on the course of the precipitation. For the stoichiometric conditions, a typical trend is observed although partial sedimentation occurs after 6 hours (by eye). Particles with typical size 14 nm (extracted from SAXS fitting) are already formed after 2 hours while crystallization process is still in progress (Figure 5 and Figures S12, S13). We observe on the patterns recorded between 2 and 6 hours diffraction peaks characteristics of intermediate compounds. We attributed them to the oxalic acid and to an amorphous phase, revealed for excess conditions in the *ex-situ* study (Figure 4). The Bragg peaks centered at 0.97 Å^{-1} and 1.95 Å^{-1} (see Figure S8) (related to the oxalic acid) and a broad peak at 1.18 Å^{-1} (related to an intermediate amorphous phase) appear first. Then their intensities decrease with increasing time (Figure 5 and 6), explaining while they were not observable on Figure 4 for *ex situ* conditions. Simultaneously, the peaks centered at 0.92 Å^{-1}, 0.94 Å^{-1}, and

0.61 Å^{-1} (and others peaks) which are characteristic of the cerium oxalate structure appear and their intensities increase as the time increases (Figure 5 and 6 and S12). Hence, oxalic acid and amorphous phase present in the first stage of the precipitation are consumed during the cerium oxalate crystal formation.
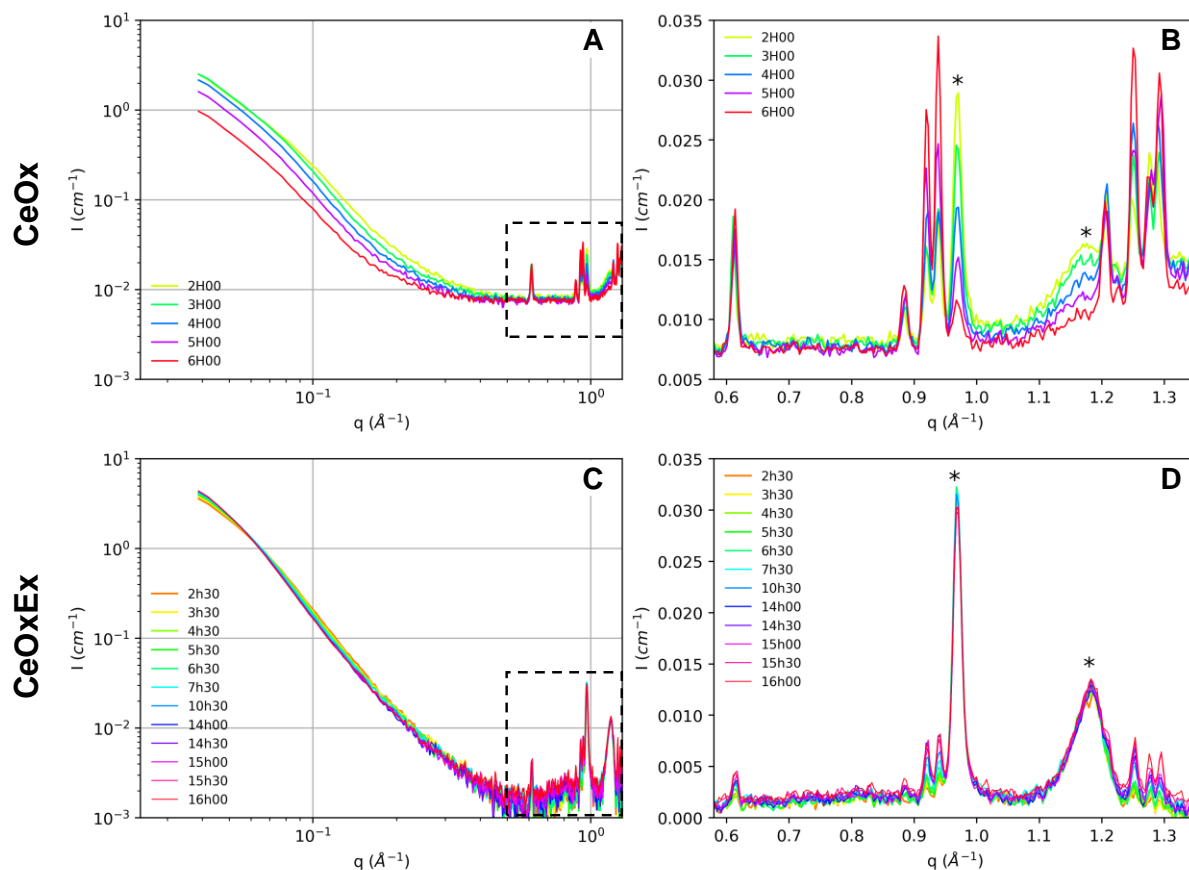

Figure 5. SAXS kinetics of cerium oxalate formation for (A, B) stoichiometric and (C, D) excess oxalic conditions in **Tern1** solvent. (A, C) log-log scale and (B, D) linear scale with a zoom on the Bragg peak region. The symbol (*) indicates the first visible peaks which intensities then decrease as the characteristic peaks of cerium oxalate crystal grow over time.

For the excess oxalic conditions, the *in situ* SAXS kinetic only shows a slight evolution over the monitored time (Figure 6 and Figures S12 and S13). In the low q region, the signature of formed particles, of size 10 nm, is present with slight increase with time. In the large q-range, intense Bragg peaks related to the intermediate compounds are visible in coexistence with low

intensity Bragg peaks typical of the cerium oxalate crystals (Figure S9). This slow evolution is consistent with the *ex situ* experiments.

For both conditions (stoichiometric and excess of oxalic acid) the particles are rapidly formed, evidenced by both the white color appearing immediately after mixing the reagents, and the intensity of the scattering at low q in the SAXS patterns (> 3 cm^{-1} after 1h), but the crystallization process is slow (evolution over hours), in particular for excess oxalic acid conditions (evolution over days) (see Figure 6, Figure S12). The particles size extracted from SAXS fitting indicates a slight evolution of the size while crystallization progresses (Figure S13). These observations are consistent with the formation of an amorphous phase in coexistence with the crystal in formation, as already observed for other crystallization processes [35]. The formation of an intermediate amorphous phase prior to the crystallization process of cerium oxalate, was reported in water, where reaction time is typically of seconds [36, 37]. However, while in water the amorphous phase is a transient intermediate phase, in the ternary system it is stabilized for a longer time (hours). In ternary solvent Tern1, the presence of oxalic acid crystals in coexistence with the cerium oxalate crystals is also visible for both conditions.
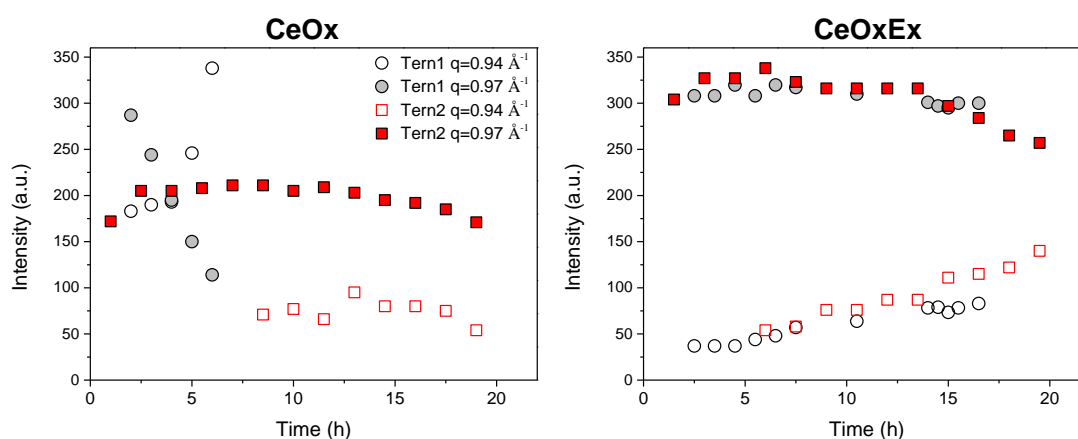

Figure 6. Bragg peak evolution versus time for **Tern1** and **Tern2** for stoichiometric and excess conditions. Cerium oxalate crystal formation is indicated by the peak at 0,94 Å^{-1} and the evolution of the transient phase by the peak at 0,97 Å^{-1}.

On the mechanisms affecting the precipitation process in water-poor ternary solvents

The amount of water in the composition of the ternary solvent is expected to impact the arrangement of the final structure of cerium oxalate crystals [22]. Based on the ternary phase diagram (Figure 1), we moved upward from primary ternary solvent Tern1 to Tern2 by dividing by 2 the concentration of water in the system.

Direct observations. In the case of solvent with the lower water content, Tern2, the mixture turned into a gel several minutes after mixing the solutions containing cerium nitrate and oxalic acid. At the end of the reaction, the gel has disappeared, and the solution is transparent with sedimented particles at the bottom.
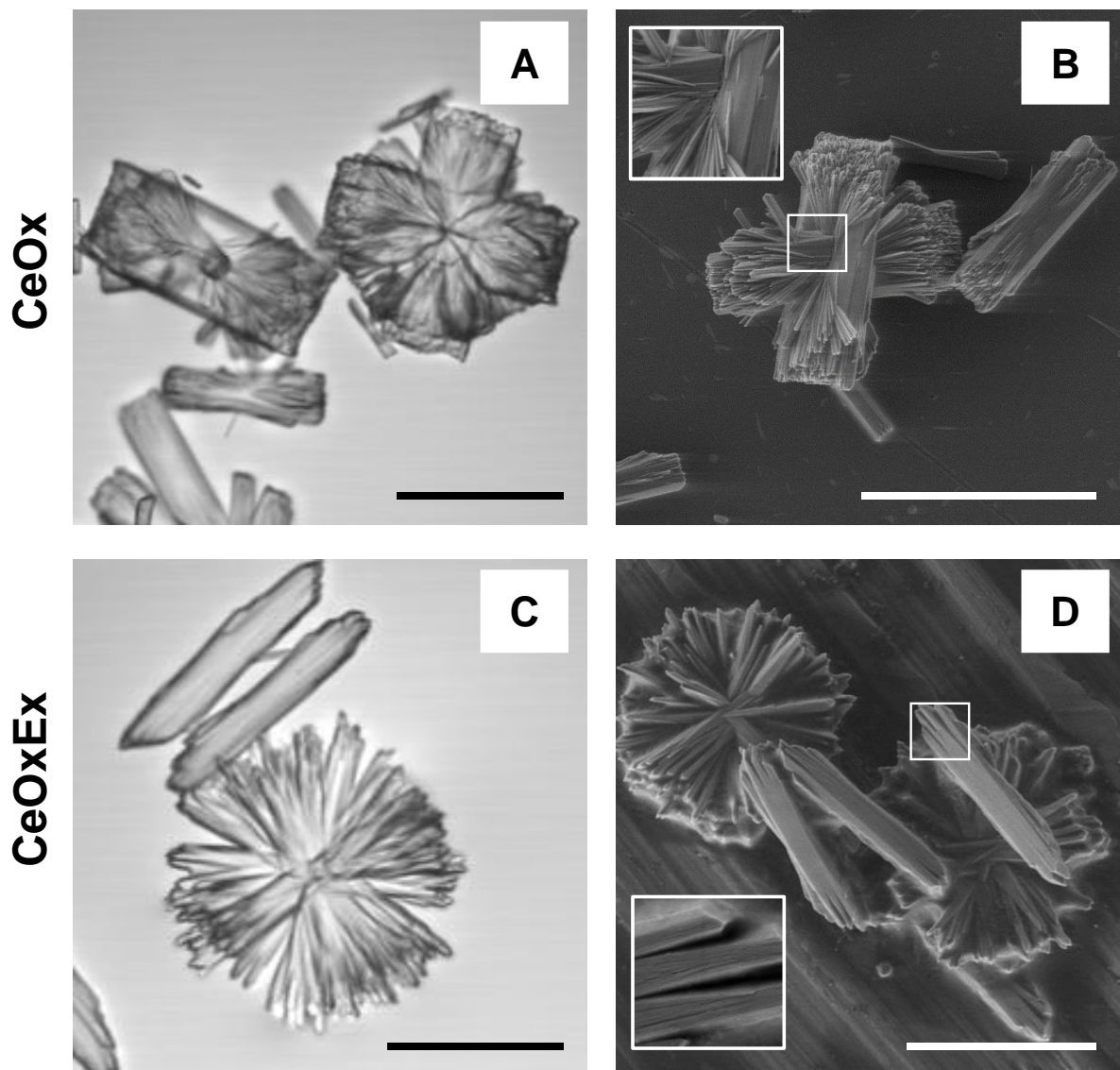
Figure 7. Optical microscopy (A, C) and environmental electron scanning microscopy (ESEM) (B, D) images of final morphology of the cerium oxalate particles under stoichiometric conditions (A, B) and excess of oxalic acid (C, D) in ternary solvent **Tern2**, i.e., after total sedimentation of the powder in the solution with 500 µl/500µl of each reagent at room temperature, i.e., ≈10 days for stoichiometric condition and ≈16 days in the excess of oxalic acid, respectively. Scale bars are 50µm.

For the same reactant concentration, the morphology of the sedimented particles formed in the Tern2 solvent (Figure 7) is not the same than the morphology of the particles formed in the Tern1 system (Figure 2). We can recognize the differences between stoichiometric conditions and excess of oxalic acid already observed in Tern1, with the appearance of wide, compact

elements (Figure 7 A, B) and thin, long elements in all the directions (Figure 7 C, D), respectively. However, in Tern2 system, the final products are denser than in Tern1, suggesting a strong effect of the water scarcity on the course of the reaction. At last, the particles grown in Tern2 solvent are 1.5 to 2 times bigger (d ≈ 50 µm) than the one grown in Tern1 solvent (d ≈ 30 µm), and the platelets assembly exhibiting higher branching is more randomly distributed.

Localization of water in the cerium oxalate particle assemblies. The water-distribution during the synthesis have been monitored by confocal microscopy technique using a fluorescent probe (Alexa Fluor™ 555 Carboxylic Acid) which is soluble in water and not soluble in the octanol phase. This probe is used to determine precisely the location of the water molecules within the cerium oxalate particles assemblies (see Experimental section, Optical microscopy part).

For stoichiometric conditions in the Tern1 system after complete sedimentation, all the oxalic acid is incorporated in the crystal, to achieve stoichiometric proportions. The fluorophores are visible only on the aggregated structures, while isolated crystals remain "black" (Figure 8 compare A and B).

On the contrary, in the case of an oxalic acid excess, fluorophore species remain visible everywhere in the image revealing that hydrated compounds are homogenously dispersed in the octanol phase. At the end of the reaction, only the unreacted oxalic acid could be found in the octanol phase. It is likely that the colorant is bounded to hydrated oxalic acid by hydrogen bonding or by forming a catanionic compound (between amine group from Alexa 555 and acid function of oxalic acid). The aggregated structures in the shape of "sea urchins" or snowflakes remain "black", and only platelets with free facets showed the presence of fluorescent dye (Figure 8 compare C and D). This difference could indicate a partition coefficient of the fluorophore between free hydrated oxalic acid and hydrated cerium oxalate particles.

Analogous phenomenon was observed for Tern2 system for both stoichiometric and oxalic acid excess conditions (data not shown).
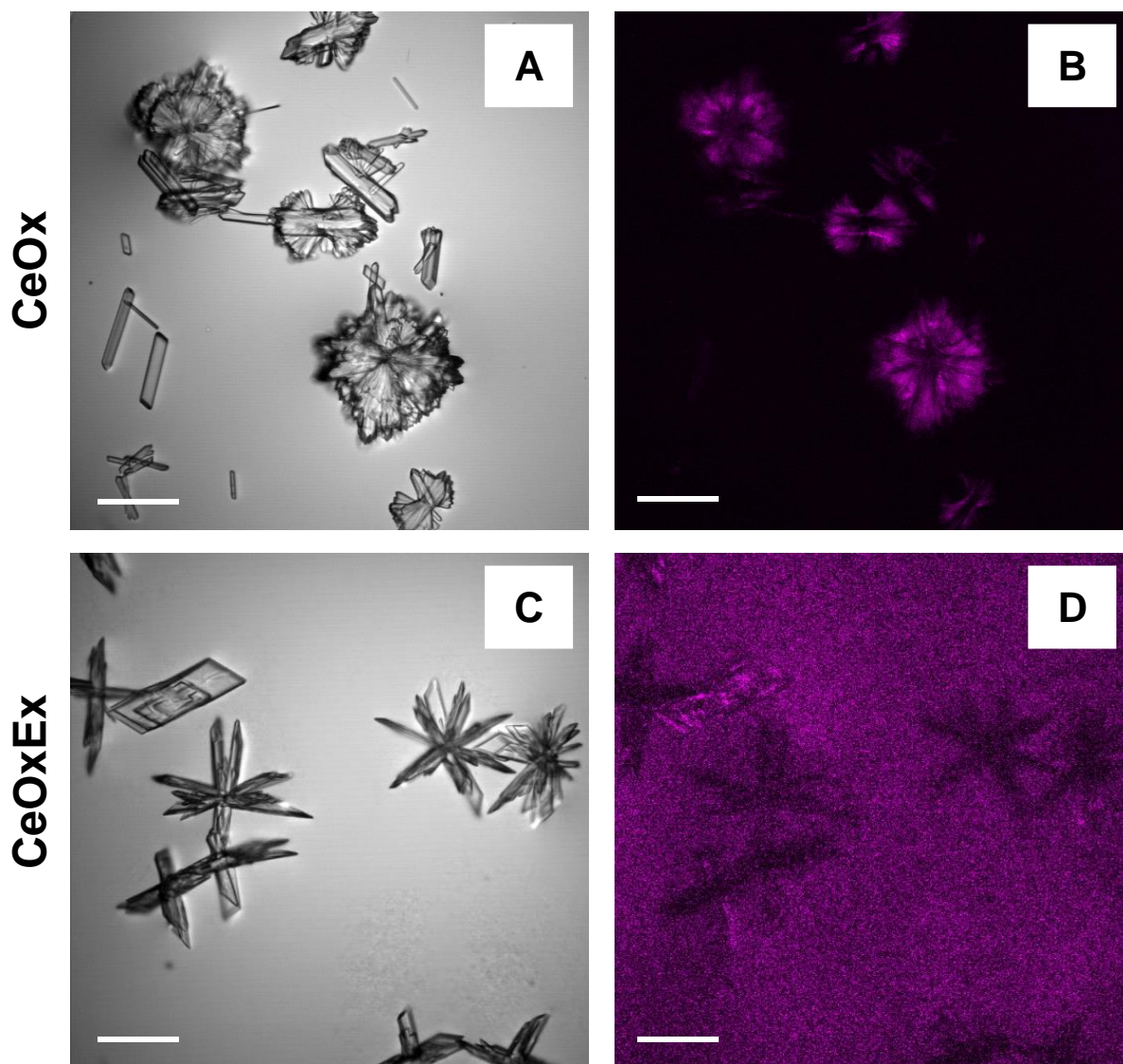
Figure 8. Images of confocal microscopy of the cerium oxalate particles after complete sedimentation under stoichiometric conditions (A, B) and excess of oxalic acid (C, D) in ternary solvent **Tern1.** Molecular probe Alexa 555 is soluble in water (appears in pink in the confocal pictures B, D) but not soluble in the octanol phase. Scale bars are 50 μm.

<u>Growth kinetics of Cerium Oxalate in Tern2.</u> In order to highlight the role of water and excess of oxalic acid in the control of the cerium oxalate morphology, SAXS monitoring of crystal

growth in the Tern2 system was performed for the first 19 hours after mixing of the reactive solutions. The results are reported in Figure 9.

As for Tern1 system, the residual signal from nanostructured ternary solvent was subtracted from each curve acquired during the kinetic experiment (see Figure S7 for comparison between nanostructured ternary solvent and reactive solution signals). The variations of the WAXS spectra as a function of ageing time are reported in Figure 9 for the two different conditions (stoichiometric and excess of oxalic acid) in Tern2 system. As for Tern1, a large scattering signal is observed in the low q-range 1 hour (respectively 1h30) after the mixing of the reactant solutions for stoichiometric (respectively excess) conditions, hence indicating the formation of particles in the solution before their complete crystallization.
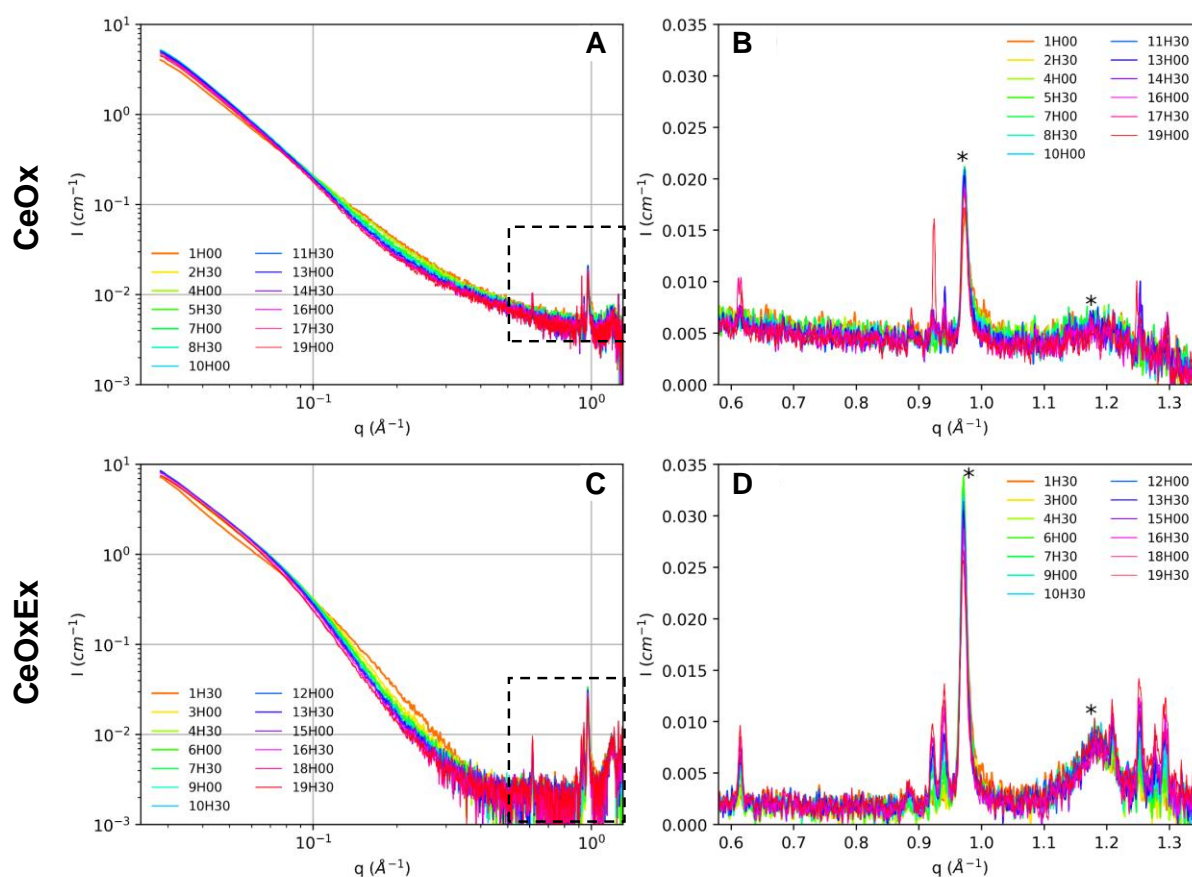
Figure 9. WAXS data of the cerium oxalate particles in (A, B) stoichiometric conditions and (C, D) excess of oxalic acid in ternary solvent **Tern2**. (A, C) log-log scale and (B, D) linear scale with zoom

on Bragg peak region. The symbol (*) indicates the first visible peaks – (oxalic acid and amorphous phase) which decrease over time as the characteristic peaks of cerium oxalate grow.

The slope at small angle is around 2.5 for the two curves (2.3 for CeOx and 2.7 for CeOxEx) but extends on a larger q domain for the CeOx case. This indicates that larger objects are formed during the experiment performed in the CeOxEx conditions, than during the experiment performed in the CeOx conditions. Fitting the data by a Beaucage model (see supporting information) confirms this difference for the primary constitutive particles embedded in a bigger grain (16 nm for stoichiometric conditions vs 20 nm for excess conditions) (Figure S13). These small characteristic sizes compared to the particle size (> 3µm) highlighted by optical microscopy and ESEM observations indicate that the precipitates exhibit a hierarchical structure.

In each case, the Bragg peak typical of oxalic acid at 0.97Å^{-1} is visible after 1 hour (Figures 9, S10 and S11). For stoichiometric conditions, some cerium oxalate Bragg peaks are only visible after 8h30 (mainly at 0.92 Å^{-1}) and after 13 h (mainly at 0.94 Å^{-1}), and they remain very smooth while the Bragg peak at 0.97 Å^{-1} slightly decreases with time after 13 h (Figure 6, Figures S10 and S12). For Tern2, the crystallization process in stoichiometric conditions is considerably slowed down compared to Tern1 (Figure 6, Figure S12), but evolves through the same intermediate structures.

For conditions corresponding to an excess of oxalic acid, the Bragg peaks increase and become more intense slightly faster than for the stoichiometric CeOx case (Figure 6, Figure S12). The crystallization kinetics are faster when oxalic acid is in excess although slower than in Tern1 conditions. This kinetic behavior is opposite to the one observed in Tern1 conditions, where the excess of oxalic acid slows down the crystallization process of cerium oxalate.

<u>Comparison of the different effects.</u> The final morphology of cerium oxalate particles is highly dependent on both the composition of the ternary solvent and the stoichiometric conditions of oxalic acid (see figure 10 for a summarized scheme of the different effects).

- Regardless of the solvent used, increasing the excess of oxalic acid over the stoichiometric condition increases the size and the branching of the particles. This effect is exacerbated in low water solvents where the crystal morphology switches from massive platelet, possibly assembled in compact crosses when Ce is in excess, to regular fans and up to multibranch urchins as oxalic acid excess increases.

- Whatever the reagent concentrations, the cerium oxalate precipitation passes through the formation of an amorphous phase, the crystallization of which can take from a few seconds [36, 37] to a few hours, or even days, depending on the stoichiometry and the water content of the solvent.

- The course of the reaction is hence modified by the water content or/and the cerium to oxalic acid ratio. Water acts both as a solvent and as a reactant in the precipitation reaction, therefore, decreasing the water content has a key role on the kinetics of the reaction and on the final morphology of the particles. The comparison of Tern1 and Tern2 SAXS data indicates that reducing the water content in the ternary solvent decreases the kinetics of the cerium oxalate crystallization reaction.

<u>Possible mechanisms.</u> For the synthesis in ternary system, the faces that grow are the ones where water is adsorbed (individual platelets and fans branches, no water is observed along the thin rods of the branched urchins). This results in compact and thick particles consisting of an assembly of layers stacked in the direction perpendicular to the direction of anisotropic, or consisting of a dense branching bundle of needles, depending on the oxalic acid concentration. Indeed, when the water content in the solvent is decreased, the compactness of the particles is increased, and this also results in larger size crystals.

The amount of oxalic acid that is brought in the solution during the reaction has a strong impact on the morphology. Whatever the water content, increasing the oxalic acid content to over-stoichiometric conditions leads to the formation of multi-branched crosses or sea urchin/star-like morphologies (Figure 2). Their formation is a slow process with first the formation of intermediate stable structures one of which is related to the oxalic acid that coexists with the cerium oxalate crystal in formation. It is remarkable that this intermediate compound, that is stable in excess of oxalic acid conditions, is also present in stoichiometric conditions, although final morphologies are different and that all the oxalic acid is supposed to be consumed during the cerium oxalate crystals formation. This intermediate structure indicates two important points: i/ a competition between water and oxalic acid in the precipitation process, and ii/ the stabilization of the amorphous phase by this intermediate oxalic acid structure.

As mentioned in the Introduction part, previous studies have shown the particular role of complex solution in modulating the morphology of cerium oxalate, either by confinement or by chemically modifying the growing particles neighborhood. For cerium oxalate nanoparticles synthetized through microemulsion route, He observed that the increase of the water content and of the temperature results in bigger particles, and that particle's formation mainly followed the coalescence-split mechanism [19]. Sun *et al.* showed that the morphology of tin oxalate changed from sphere-like aggregates to flower-like aggregates, when reducing by 4 times the water content in the precipitation water/ethanol/PEG mixture [38]. Similar morphological variations have been observed by Fu *et al.* during sodium oxalate precipitation in the presence of different anions or polymers [39, 40]. The formation of compact structures can result from new layers developed by branching along the growth direction and Fu *et al.* have identified that the crosses morphologies are related to the penetration twins. While the multistep branching growth has been explained by the so-called "non-crystallographic" crystal branching model

which depends on the supersaturation, defects in the crystal, relative kinetic growth of facets and diffusion supply [41].

Besides, biphasic solvents as water/alcohol mixtures are known to be nanostructured with a water network embedded in the alkyl chain of the alcohol [42, 43]. This allows low water fractions to be achieved, and can modify the reactivity and diffusion of reactive species. The confinement of water in ternary systems restricts the reactants diffusion, and this is likely to reduce the area of the crystals growth and confines their final morphology. In our study, the variation in morphology is achieved by modifying the composition and the nanostructuring of the ternary solution, in conjunction with the so-called surfactant-free microemulsions [24] obtained by mixtures of alcohol and water. Pang *et al.* have already observed that the cerium oxalate precipitation in glycol/water solvent lead to a more compact structure (bricks-like) than reaction in glycerine/water (plate-like structure) [44]. Jehannin *et al.* related the structure of the ternary alcohol solution (water/propanediol/octanol) with the particle's morphology, with an aggregation of particles induced by the decrease in the water fraction [22]. Complementing the results of this previous study, we identified here the multi- twinning aspect of the particles for lower reactant concentrations (Figure 2, 3 and 7).

Additionally, the transport properties are also affected by the solvent structuration: viscosity is higher and correlatively, diffusion coefficient are lower. The formation of the gel in the Tern2 conditions is consistent with the appearance of pendular networks observed in solid/water/oil systems where particles are wetted by the minority phase only (here water) [45]. The geometry of such pendular networks consists of solid particles connected two-by-two by capillary bridges. The only difference with typical solid dispersions in liquid/liquid systems, is that in our case the particles are synthetized in the water poor ternary system and not introduced as preformed particles. With the formation of the gel, the viscosity of the mixture is further increased, and the particles are locked into the resulting sort of polymeric network [46]. This is

responsible for the spectacular slowdown of the precipitation reaction compared to Tern1 conditions. However, after several days, the gel has disappeared, and the solution became transparent with sedimented particles at the bottom. Again, this result is consistent with initial formation of a yield-stress fluid, as the strength of the capillary bridges decreases with increased particle size [47], e.g. in our case while bigger aggregates are formed.
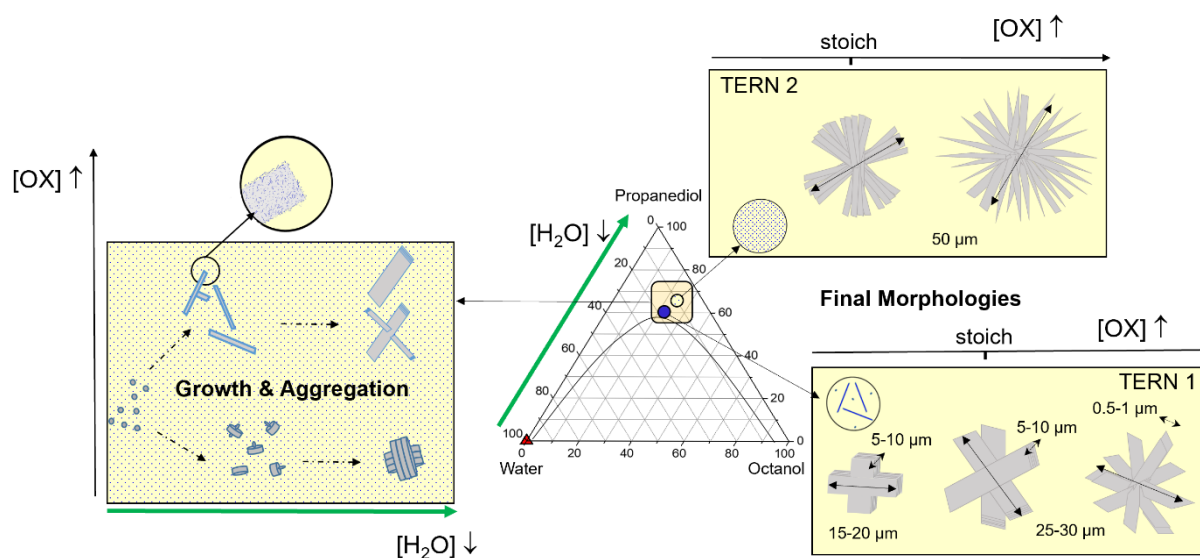
Figure 10. Scheme summarizing the effects of two parameters (water and oxalic acid concentrations) on the morphology of cerium oxalate precipitated in a surfactant free emulsion.

Conclusion

In this article, cerium oxalate particles were precipitated in ternary solvent (water/hydrotrope/lipotrope) for stoichiometric and sub or over stoichiometric conditions. Decreasing the water content in the nanostructured solvent increases the crystallization reaction time and leads to the formation of compact structures of cerium oxalate particles, with a brick-like shape embedded in a cross or fan-shape. Water constraints impose a confinement of the growth stage of the reaction.

Oxalic acid plays a key role in the final morphology. Reaction with excess oxalic acid conditions produces bundles of needles assembled in a sea urchin shape, with however a higher compact organization with decreasing water content.

For all the investigated conditions, the particles first precipitate through the same amorphous state prior to the crystallization. Reducing the water content stabilizes the intermediate state of the particles, whatever the oxalic acid stoichiometry. However, this amorphous state is further stabilized under oxalic acid excess conditions, indicating a competition between water and oxalic acid in the precipitation process.

The particles of cerium oxalate synthesized in different nanostructured solutions have different morphologies. The obtained morphology with cross-shape (stoichiometric) and branching (excess oxalic acid) results from intrinsic defects in the crystal. The originality here is to modulate the morphology by a simple variation in the composition of the ternary alcohol solution (also called surfactant free microemulsion) which opens new direction in terms of easy manipulation, solvent recycling and morphological control (single particles to agglomerates) in precipitation reactions.

References

[1] L. Treccani, T. Yvonne Klein, F. Meder, K. Pardun, K. Rezwan, Functionalized ceramics for biomedical, biotechnological and environmental applications, Acta Biomaterialia, 9 (2013) 7115-7150.

[2] C. Tamain, B. Arab Chapelet, M. Rivenet, F. Abraham, R. Caraballo, S. Grandjean, Crystal Growth and First Crystallographic Characterization of Mixed Uranium(IV)–Plutonium(III) Oxalates, Inorganic Chemistry, 52 (2013) 4941-4949.

[3] K. Binnemans, P.T. Jones, B. Blanpain, T. Van Gerven, Y. Yang, A. Walton, M. Buchert, Recycling of rare earths: a critical review, Journal of Cleaner Production, 51 (2013) 1-22.

[4] S. Mochizuki, F. Fujishiro, The photoluminescence properties and reversible photoinduced spectral change of CeO2 bulk, film and nanocrystals, physica status solidi (b), 246 (2009) 2320-2328.

[5] B.A. Rzigalinski, C.S. Carfagna, Cerium Oxide Nanoparticles: Potential for Revolutionizing Treatment of Diseases, in: Nanotechnology Characterization Tools for Environment, Health, and Safety, Springer, 2019, pp. 217-243.

[6] N.V. Skorodumova, S.I. Simak, B.I. Lundqvist, I.A. Abrikosov, B. Johansson, Quantum Origin of the Oxygen Storage Capability of Ceria, Physical Review Letters, 89 (2002) 166601.

[7] Y. Altaş, H. Tel, Structural and thermal investigations on cerium oxalate and derived oxide powders for the preparation of (Th,Ce)O2 pellets, Journal of Nuclear Materials, 298 (2001) 316-320.

[8] W. Liu, L. Feng, C. Zhang, H. Yang, J. Guo, X. Liu, X. Zhang, Y. Yang, A facile hydrothermal synthesis of 3D flowerlike CeO2via a cerium oxalate precursor, Journal of Materials Chemistry A, 1 (2013) 6942-6948.

[9] G. Vimal, K.P. Mani, P.R. Biju, C. Joseph, N.V. Unnikrishnan, M.A. Ittyachen, Structural studies and luminescence properties of CeO2:Eu3+ nanophosphors synthesized by oxalate precursor method, Applied Nanoscience, 5 (2015) 837-846.

[10] G. Zhang, Z. Shen, M. Liu, C. Guo, P. Sun, Z. Yuan, B. Li, D. Ding, T. Chen, Synthesis and Characterization of Mesoporous Ceria with Hierarchical Nanoarchitecture Controlled by Amino Acids, The Journal of Physical Chemistry B, 110 (2006) 25782-25790.

[11] I. Rodríguez-Ruiz, S. Teychené, Y. Vitry, B. Biscans, S. Charton, Thermodynamic modeling of neodymium and cerium oxalates reactive precipitation in concentrated nitric acid media, Chemical Engineering Science, 183 (2018) 20-25.

[12] S. Kawaguchi, Variety in coordination modes of ligands in metal complexes, Springer Science & Business Media, 2012.

[13] T.A. Witten, L.M. Sander, Diffusion-limited aggregation, Physical Review B, 27 (1983) 5686-5697.

[14] V. Tyrpekl, P. Markova, M. Dopita, P. Brázda, M.A. Vacca, Cerium Oxalate Morphotypes: Synthesis and Conversion into Nanocrystalline Oxide, Inorganic Chemistry, 58 (2019) 10111-10118.

[15] A. Ansari, C. Jones, E. Henry, J. Hofrichter, W. Eaton, The role of solvent viscosity in the dynamics of protein conformational changes, Science, 256 (1992) 1796-1798.

[16] E. Gómez, B. González, N. Calvar, Á. Domínguez, Excess molar properties of ternary system (ethanol+water+1,3-dimethylimidazolium methylsulphate) and its binary mixtures at several temperatures, The Journal of Chemical Thermodynamics, 40 (2008) 1208-1216.

[17] M.V. John, M.A. Ittyachen, Studies on Ce2(C2O4)3·nH2O crystals grown in hydro-silica gel, Bulletin of Materials Science, 21 (1998) 387-391.

[18] M. Mary C, V. G, K.P. Mani, G. Jose, B. P.R, C. Joseph, U. N.V, I. M.A, Growth and characterization of Sm3+ doped cerium oxalate single crystals, Journal of Materials Research and Technology, 5 (2016) 268-274.

[19] Y. He, Study on the formation mechanism of cerium oxalate nanoparticles from the coupling route of homogeneous precipitation with microemulsion, Materials Letters, 59 (2005) 3010-3013.

[20] S. Vaidya, J. Ahmed, A.K. Ganguli, Controlled synthesis of nanomaterials using reverse micelles, Defence science journal, 58 (2008) 531-544.

[21] K.V. Krishnamurty, G.M. Harris, The Chemistry of the Metal Oxalato Complexes, Chemical Reviews, 61 (1961) 213-246.

[22] M. Jehannin, S. Charton, B. Corso, H. Möhwald, H. Riegler, T. Zemb, Structured solvent effects on precipitation, Colloid and Polymer Science, 295 (2017) 1817-1826.

[23] G.D. Smith, C.E. Donelan, R.E. Barden, Oil-continuous microemulsions composed of hexane, water, and 2-propanol, Journal of Colloid and Interface Science, 60 (1977) 488-496.

[24] S. Schöttl, J. Marcus, O. Diat, D. Touraud, W. Kunz, T. Zemb, D. Horinek, Emergence of surfactant-free micelles from ternary solutions, Chemical Science, 5 (2014) 2949-2954.

[25] T.N. Zemb, M. Klossek, T. Lopian, J. Marcus, S. Schöettl, D. Horinek, S.F. Prevost, D. Touraud, O. Diat, S. Marčelja, W. Kunz, How to explain microemulsions formed by solvent mixtures without conventional surfactants, Proceedings of the National Academy of Sciences, 113 (2016) 4260-4265.

[26] W. Hou, J. Xu, Surfactant-free microemulsions, Current Opinion in Colloid & Interface Science, 25 (2016) 67-74.

[27] Y. Zhang, X. Chen, B. Zhu, Y. Zhou, X. Liu, C. Yang, Temperature-Switchable Surfactant-Free Microemulsion, Langmuir, 36 (2020) 7356-7364.

[28] M. Pileni, Reverse micelles as microreactors, The Journal of physical chemistry, 97 (1993) 6961-6973.

[29] T. Lopian, S. Schöttl, S. Prévost, S. Pellet-Rostaing, D. Horinek, W. Kunz, T. Zemb, Morphologies Observed in Ultraflexible Microemulsions with and without the Presence of a Strong Acid, ACS Central Science, 2 (2016) 467-475.

[30] M. Jehannin, About the role of physico-chemical properties and hydrodynamics on the progress of a precipitation reaction: the case of cerium oxalate particles produced during coalescence of drops, in, 2015.

[31] D. Stokes, Principles and practice of variable pressure/environmental scanning electron microscopy (VP-ESEM), John Wiley & Sons, 2008.

[32] Python for Small Angle X-ray Scattering data treatment, p. 3.234, https://pypi.org/project/pySAXS/, in.

[33] V. Geertsen, E. Barruet, F. Gobeaux, J.-L. Lacour, O. Taché, Contribution to Accurate Spherical Gold Nanoparticle Size Determination by Single-Particle Inductively Coupled Mass Spectrometry: A Comparison with Small-Angle X-ray Scattering, Analytical Chemistry, 90 (2018) 9742-9750.

[34] M. Tomšič, M. Bešter-Rogač, A. Jamnik, W. Kunz, D. Touraud, A. Bergmann, O. Glatter, Nonionic Surfactant Brij 35 in Water and in Various Simple Alcohols: Structural Investigations by Small-Angle X-ray Scattering and Dynamic Light Scattering, The Journal of Physical Chemistry B, 108 (2004) 7021-7032.

[35] B. Fleury, M.-A. Neouze, J.-M. Guigner, N. Menguy, O. Spalla, T. Gacoin, D. Carriere, Amorphous to Crystal Conversion as a Mechanism Governing the Structure of Luminescent YVO4:Eu Nanoparticles, ACS Nano, 8 (2014) 2602-2608.

[36] I. Rodríguez-Ruiz, S. Charton, D. Radajewski, T. Bizien, S. Teychené, Ultra-fast precipitation of transient amorphous cerium oxalate in concentrated nitric acid media, CrystEngComm, 20 (2018) 3302-3307.

[37] T. Lange, S. Charton, T. Bizien, F. Testard, F. Malloggi, OSTE+ for in situ SAXS analysis with droplet microfluidic devices, Lab on a Chip, 20 (2020) 2990-3000.

[38] H. Sun, S.-Z. Kang, J. Mu, A Simple Precursor-Assisted Preparation of Flowerlike SnO2 Nanostructures, Journal of Dispersion Science and Technology, 30 (2009) 466-471.

[39] W. Fu, J. Vaughan, A. Gillespie, Effects of Inorganic Anions on the Morphology of Sodium Oxalate Crystallized from Highly Alkaline Solutions, Crystal Growth & Design, 14 (2014) 1972-1980.

[40] W. Fu, J. Vaughan, A. Gillespie, N.M. Aroff, Mechanisms of Polyacrylate Modified Sodium Oxalate Crystallization from Highly Alkaline Solutions, Crystal Growth & Design, 16 (2016) 1519-1530.

[41] A. Thomas, E. Rosseeva, O. Hochrein, W. Carrillo-Cabrera, P. Simon, P. Duchstein, D. Zahn, R. Kniep, Mimicking the Growth of a Pathologic Biomineral: Shape Development and Structures of Calcium Oxalate Dihydrate in the Presence of Polyacrylic Acid, Chemistry – A European Journal, 18 (2012) 4000-4009.

[42] B. Abécassis, F. Testard, T. Zemb, L. Berthon, C. Madic, Effect of n-Octanol on the Structure at the Supramolecular Scale of Concentrated Dimethyldioctylhexylethoxymalonamide Extractant Solutions, Langmuir, 19 (2003) 6638-6644.

[43] G. Cevc, I. Berts, S.F. Fischer, J.O. Rädler, B. Nickel, Nanostructures in n-Octanol Equilibrated with Additives and/or Water, Langmuir, 34 (2018) 6285-6295.

[44] H. Pang, C. Chen, Facile synthesis of cerium oxide nanostructures for rechargeable lithium battery electrode materials, RSC Advances, 4 (2014) 14872-14878.

[45] S.J. Heidlebaugh, T. Domenech, S.V. Iasella, S.S. Velankar, Aggregation and Separation in Ternary Particle/Oil/Water Systems with Fully Wettable Particles, Langmuir, 30 (2014) 63-74.

[46] C. Noirjean, C. Vancaeyzeele, S. Bourcier, F. Testard, F. Vidal, D. Carriere, O. Fichet, Nanostructure Changes upon Polymerization of Aqueous and Organic Phases in Organized Mixtures, Langmuir, 32 (2016) 10104-10112.

[47] E. Koos, J. Johannsmeier, L. Schwebler, N. Willenbacher, Tuning suspension rheology using capillary forces, Soft Matter, 8 (2012) 6620-6628.

For Table of Contents Only